Osteotropic therapy via targeted Layer-by-Layer nanoparticles

Stephen W. Morton[‡], **Nisarg J. Shah**[‡], **Mohiuddin A. Quadir**, **Zhou J. Deng**, **Zhiyong Poon**, and **Paula T. Hammond**

The David H. Koch Institute for Integrative Cancer Research, Department of Chemical Engineering, Institute for Soldier Nanotechnologies, 77 Massachusetts Avenue, Cambridge, MA 02139

Paula T. Hammond: hammond@mit.edu

Abstract

Current treatment options for debilitating bone diseases such as osteosarcoma, osteoporosis, and bone metastatic cancer are suboptimal and have low efficacy. New treatment options for these pathologies require targeted therapy that maximizes exposure to the diseased tissue and minimizes off-target side effects. This work investigates an approach for generating functional and targeted drug carriers specifically for treating primary osteosarcoma, a disease in which recurrence is common and the cure rate has remained around 20%. Our approach utilizes the modularity of Layer-by-Layer (LbL) assembly to generate tissue-specific drug carriers for systemic administration. This is accomplished via surface modification of drug-loaded nanoparticles with an aqueous polyelectrolyte, poly(acrylic acid) (PAA), side-chain functionalized with alendronate, a potent clinically-used bisphosphonate. Nanoparticles coated with PAA-Alendronate are observed to bind and internalize rapidly in human osteosarcoma 143B cells. Encapsulation of doxorubicin, a front-line chemotherapeutic, in an LbL-targeted liposome demonstrates potent toxicity *in vitro*. Active targeting of 143B xenografts in NCR nude mice with the LbL-targeted doxorubicin liposomes promotes enhanced, prolonged tumor accumulation and significantly improved efficacy. This report represents a tunable approach towards the synthesis of drug carriers, in which LbL can enable surface modification of nanoparticles for tissue-specific targeting and treatment.

Keywords

Layer-by-Layer; cancer therapy; bone; bisphosphonate

Correspondence to: Paula T. Hammond, hammond@mit.edu.

‡Equally contributing authors

The authors wish to dedicate this paper to the memory of Officer Sean Collier, for his caring service to the MIT community and for his sacrifice.

Supporting Information

Supporting Information is available online from the Wiley Online Library or from the author.

1. Introduction

The development, maintenance, and repair of bone require cell-mediated remodeling to sustain the structural integrity of the tissue. Disturbances in the physiological processes of osteoblast-mediated bone deposition and osteoclast-mediated bone resorption are observed in many bone-related disease states, such as osteosarcoma, cancer metastasis to bone, osteoporosis, and Paget's disease of the bone.[1] Several therapies have been developed to combat these pathologies;[1–2] however, the clinical outcomes for patients with these diseases continue to be very poor. The arsenal of available agents to treat patients has not made any substantial impact in improving their survival, and new methods for therapy are critical. Engineering a robust delivery platform with bone-tissue level specificity to treat these diseases can improve therapeutic efficacy, lower systemic toxicity, and improve disease management.

Significant fundamental work in the area of bone biology has uncovered the potential of bone-specific agents, such as bisphosphonates.[2b, 3] These compounds act as pharmacophores, whereby the pyrophosphate-like structure coordinates calcium ions within the hydroxyapatite mineral in bone with high affinity and specificity. Accumulation of bisphosphonates further promotes inhibition of bone resorption by inducing apoptosis in osteoclasts that are responsible for this action. As such, this class of pharmaceutics is a potent drug for promoting homeostasis between osteoclast and osteoblast activity in, for example, osteoporosis, while also promoting tissue-specific binding and localization.

Bone targeting systems[4] have been synthesized to utilize the specificity of a variety of ligands, including bisphosphonates, tetracycline and derivatives, sialic acid, and bio-inspired materials containing similar functionalities[2b]; however, systems capable of therapeutic delivery for treatment of bone-related diseases remain limited. Towards this end, the modularity of Layer-by-Layer (LbL)-functionalized nanomedicine systems[5] presents an attractive opportunity to incorporate these bone-specific, highly water-soluble ligands on the surface of nanotechnology for targeted drug delivery. LbL assembly[6] is a highly controlled approach to iteratively deposit materials and functionalize the surface of virtually any substrate on the basis of complementary interactions, such as electrostatics. This method allows for tunable, nanoscale precision over system design, allowing for the construction of a customizable therapeutic delivery platform[5i, 7]. Recent work has demonstrated the potential for LbL nanoparticle systems to promote improved pharmacokinetics and biodistribution of the carrier and drug *in vivo*,[8] with the ability to modulate release of encapsulated therapeutics. Complementary studies investigated tumor microenvironment cue-sensitive designs (e.g. pH-responsive[9]) that harnessed tumor hypoxia to promote enhanced localization and uptake in tumors. Further, these built-to-order systems have been recently manufactured on a scalable platform[10], demonstrating potential to mass-produce these systems with high levels of control.

In this study, we report the synthesis of tissue-targeted LbL nanoparticles, specifically manufactured to hone in on bone tissue. To achieve this, a polyelectrolyte, poly(acrylic acid) (PAA), was functionalized with a bisphosphonate, alendronate, and subsequently electrostatically-assembled in a nanoparticle coating. The functionalized particles

accumulated in subcutaneous 143B osteosarcoma xenografts, where they delivered their payload, doxorubicin, in a mouse model. The targeted particles significantly attenuated tumor burden and extended animal survival, in some cases even completely eliminating tumors. The results described herein establish LbL as a modular approach to develop targeted drug carriers via adsorption of ligand-functionalized, aqueous polyelectrolytes for tissue-specific targeting, further developing these systems towards clinical application.

2. Results and Discussion

LbL-targeted nanoparticle systems were generated by covalent modification of PAA (M_v ~ 450K, Figure 1A) with alendronate (Figure 1B) at 40% functionalization of the total carboxylic groups on the PAA molecule (Figure 1C). Alendronate was coupled via its amino functional handle to PAA through an amide bond. As both of the components were water soluble, we used methyl morpholine-based water-soluble coupling agents to perform amide coupling (Figure S1). The immobilization of the molecule onto the PAA backbone was confirmed by ^{31}P and ^{1}H NMR. The functionalized PAA-Alendronate polymer was subsequently used as the polyanionic layer in LbL assembly, iteratively adsorbed on a solid nanoparticle substrate in alternation with polycationic poly-L-lysine (PLL), as schematically illustrated in Figure 1D. PAA is a well-characterized[11] weak polyanion with a high charge density and a non-erodible backbone that has been listed as an approved excipient in the FDA's Inactive Ingredient Guide and is used in clinically-approved drug formulations as a stabilizer and thickener to tune the rheological properties of the injectable or topically-applied therapeutic. As such, PAA presented a suitable material for introducing tissue specificity and targeting via alendronate functionalization.

To establish these systems as osteotropic delivery systems, initial investigations employed a 25 nm quantum dot (QD) (CdSeTe core) for imaging purposes to understand how the coating directed particle association with osteosarcoma cells (143B) *in vitro* and *in vivo*, as well as other hard tissue *in vivo*. These particles were fabricated as shown in Figure 1D, with linear film growth observed for three bilayers of (PLL/PAA-Alendronate) to a final z-average hydrodynamic diameter of 115 nm, with a PDI of 0.19, and zeta-potential of −39 mV (10 mM NaCl in DI water, 25°C; Figure S2).

Incubation of LbL-targeted QD_{705} nanoparticles with 143B cells showed significant binding and cell uptake after 2 hours at 37°C (see Figure 2A), where red is representative of QD_{705} nanoparticle fluorescence. Nanoparticle binding, on the basis of QD_{705} fluorescence, was further characterized and observed to be dose-dependent for a range of concentrations, over which little cytotoxicity (48 hour incubation) was observed, as shown in Figure 2B. The number of bilayers (1, 2, and 3, whereby 1, 2, and 3 layers of the targeted PAA-Alendronate polymer are incorporated on the particle surface) was also investigated. These results are shown Figure S3. It was observed that the *in vitro* binding affinities and cytotoxicity profile were similar across different bilayer numbers. Previous work[8b] established the improved biological performance of QD nanoparticles with 3 or more bilayers; therefore, we focused on the 3-bilayer LbL-targeted QD particles for *in vivo* assessment of targeting.

To evaluate this system *in vivo*, LbL-targeted QD_{800} nanoparticles were administered via the tail vein in NCR nude mice with ectopically induced 143B osteosarcoma xenografts. Particle distribution in live animals was tracked using whole-animal *in vivo* fluorescence imaging (Figure 3A). Immediately following administration, the particles rapidly accumulated in the bone tissue regions, particularly in the parietal region of the cranium, spinal column, and hind limb regions. At later time points, particles trafficked to the 143B xenografts, consistent with targeted interactions with the tumor matrix. Controls for uncoated, untargeted QDs and coated QDs with unconjugated PAA showed no specific affinity for hard tissue and had little to no accumulation in the xenografts, suggesting the enhanced permeation and retention effect does not account for much of this tumor localization (Figure S4). Tumor-specific accumulation was significant and observed over the course of 8 days (Figure 3B). Such a long period of accumulation may be due to the strong binding affinity between alendronate and the osteosarcoma tissue, leading to much longer residences times of the nanoparticle in the tumor. The tumors were resected after 8 days, along with necropsy of other relevant tissue, and analyzed via recovered fluorescence to investigate post-mortem particle distribution. Significant localization of particles was observed in xenografts (accounting for ~30% fluorescence recovered), relative to ~40% in the liver and smaller fractions in each of the other organs (spleen, kidneys, heart, lungs) harvested (Figure 3C, Figure S5). Accumulation in the liver is a common challenge for all nanoparticle delivery platforms, though we have shown in other work that the use of hyaluronic acid can lower accumulation considerably compared to other systems. Future work will investigate its use for introducing tissue specificity via ligand functionalization.

To visualize the biodistribution of both the coating and nanoparticle in real time, the bisphosphonate-targeted polymer, PAA-Alendronate, was labeled with a near-IR, Cy5.5 dye and adsorbed onto the surface of QD_{800} to allow for two-color *in vivo* imaging of the targeted, 3 bilayer $(PLL/PAA_{Cy5.5}\text{-Alendronate})_3$ nanoparticle. We observed co-localization of the two components – the PAA-Alendronate outer layer and the quantum dot - in the xenografts (Figure 3D, Figure S5) for up to 9 days, further substantiating these systems as serum-stable targeted platforms for delivery.

Next, we applied the coating, (PLL/PAA-Alendronate), to drug-loaded particle systems for targeted delivery and treatment of diseased tissue. For this purpose, the coatings were adapted to a liposomal carrier for use in drug delivery (Figure 4A). Initial work focused on empty, negatively-charged liposomal carriers, containing DSPC (1,2-distearoyl-*sn*-glycero-3-phosphocholine), cholesterol, and POPG (1-palmitoyl-2-oleoyl-*sn*-glycero-3-phospho-(1'-*rac*-glycerol)), functionalized with one bilayer of PLL/PAA-Al, which yielded 170 nm nanoparticles with a zeta-potential of −20 mV (Figure S6), to validate these systems for LbL-targeted delivery. Due to size considerations for systemic delivery, fabrication was truncated after a single bilayer due to the significant increase in size associated with adsorption of a single bilayer (80–90 nm per bilayer). Differences in bilayer thickness relative to films on QDs could be due to the relative fluidity of the liposomal substrate. Consistent with results for the LbL-targeted QDs, binding of the LbL-functionalized liposomes to 143B cells was observed to be dose-dependent and not apparently cytotoxic (Figure 4B). Rapid internalization after a 2 hour incubation with the 143B cells, visualized

by confocal microscopy (Figure 4C) and confirmed via flow cytometry (Figure 4D), was also observed. The high levels of red, diffuse nanoparticle fluorescence (visualized by incorporation of PLL-Cy5.5 in the LbL coating), along with a marked shift in cell-associated fluorescence observed by flow cytometry, suggested this system enabled high levels of nanoparticle binding and uptake, providing a promising platform for LbL-targeted drug delivery.

Osteosarcomas are known to be responsive to conventional chemotherapeutics, such as doxorubicin, so we next explored the incorporation of doxorubicin in the liposomal carrier for subsequent LbL functionalization. We were able to incorporate doxorubicin into stable DSPC:Cholesterol:POPG liposomes with high drug-loading efficiency (97%) at 5.5 w/w% (drug/lipid). During subsequent coating with a single bilayer of (PLL/PAA-Alendronate), no drug loss was observed, and liposomal morphology remained unchanged, as illustrated in Figure 4A. The LbL-functionalized doxorubicin-loaded liposome was characterized by a hydrodynamic diameter of approximately 210 nm in size with a zeta-potential of −20 mV, measured in 10 mM NaCl (Figure S6). The targeted liposomal carriers were found to be particularly potent against 143B cells, with high levels of toxicity over a wide-range of doxorubicin-loaded concentrations following incubation for 24 hours and 48 hours (Figure 4E), whereas the uncoated control showed about 8-fold lower levels of toxicity (Figure 4F).

Translating these systems *in vivo*, we first investigated the pharmacokinetics of the coated liposomal system in the absence of drug. Shown in Figure 5A is the circulation profile of this system on the basis of fluorescence recovery following systemic administration of the PLL-Cy5.5 labeled carriers to immune-proficient BALB/c mice. Based on a two-compartment model, the targeted carriers exhibited half-lives of 0.23 hours (fast) and 18.7 hours (slow), indicative of a stable, long-circulating system that could promote enhanced delivery of loaded therapeutics.

In tumor-bearing NCR nude mice, the same PLL-Cy5.5 labeled, targeted system was observed to accumulate in the target diseased tissue rapidly, with the ability to persist in the tumor up to the terminal point of the study - 100 hours (Figure 5B, Figure S7). Biodistribution results (Figure 5C, Figure S7) at the terminal point of this investigation further corroborated these systems as stable delivery platforms that preferentially locate in osteosarcoma xenografts at high levels (~35% on the basis of fluorescence recovery, relative to ~47% in the liver, ~7% in the kidneys). Elevated amounts of recovered fluorescence in the liver suggested that hepatic clearance is the primary means of excretion; however, the large number associated with the liver, in addition to the values reported for other tissue, is not meant to be wholly quantitative, as the data is reported as percent of the total fluorescence recovered from only the tissue collected. The relative ratios of fluorescence between tissue confirmed that we were able to achieve a high level of tumor specificity relative to the other tissue, which validated this system for further investigation towards therapeutic delivery.

After observing high levels of tumor localization for the targeted empty liposomal formulation, the efficacy of the LbL-targeted doxorubicin-loaded liposomes was evaluated against 143B osteosarcoma xenograft-bearing NCR nude mice. Initial attempts at

determining the optimal dosing regimen (drug concentration and number/timing of injections) employed a dose escalation study of serial 1 mg/kg, 2 mg/kg, and 3 mg/kg (based on doxorubicin loading) injections starting at day 10 post-tumor inoculation with each treatment separated by one week. As observed in Figure 6A, untreated osteosarcoma tumors grew beyond terminal size (diameter > 1 cm) after 19 days post-inoculation. Treated mice for both the uncoated and coated versions survived repeated dosing out to 30 days, after which comparisons in terminal tumor size were drawn. As observed visually in Figure 6A and quantified in Figure 6B, LbL-targeted doxorubicin-loaded liposome treated mice showed significantly reduced terminal tumor sizes relative to the uncoated doxorubicin-loaded liposome control (characterized by measurements on the longest x-y dimensions). This observation is consistent with enhancement of the therapeutic potency of the loaded drug due to preferential accumulation of the targeted system in the 143B xenografts.

Results from the dose escalation study indicated that a higher dose was necessary to effectively remediate the tumor. For this purpose, LbL-targeted doxorubicin-loaded liposomes were administered at a doxorubicin concentration of 5 mg/kg, along with an uncoated, drug-loaded control at the same concentration. Xenograft-bearing mice were allowed to develop tumors to an area of ~25 mm^2 [measured in the longest length and width dimensions] after which they were treated, with repeated injections one week apart for 3 total treatments until a terminal point at day 40. We observed enhanced efficacy of the LbL-targeted doxorubicin-loaded liposome, relative to the uncoated control, as determined by caliper measurements and visual inspection of the terminal point harvested xenografts (Figure 6C). Varying levels of therapeutic benefit for the targeted group were observed from complete remediation (NT – no tumor observed) to tumor maintenance (tumor reduction of 30% from day 0 on average), whereas the uncoated control group mice showed significant tumor growth (several beyond the maximum allowable tumor burden of 1 cm in diameter; growth of 550% from day 0 on average). These results highlight the capabilities of the LbL-targeted nanoparticle approach for highly effective chemotherapeutic treatment in tumor-bearing mice.

Histological analysis via a Masson’s trichrome stain of recovered osteosarcoma (143B) tumor tissue following treatment with each the targeted and untargeted doxorubicin-loaded liposomal formulations at 5 mg/kg is displayed in Figure 7. Initially, the tumor demonstrates an abundance of 143B cells (stained red) and connective tissue (stained blue) in the tumor mass (left column). Particles coated with alendronate for targeting the tumor tissue resulted in significant cell death (right column, top row). A lower level of cell death resulted in tumors with uncoated nanoparticles (right column, middle row). Virtually no change in the tumor infrastructure was observed in untreated animals (right column, bottom row). Micro-CT analysis of these tumors immediately prior to resection (Figure S8) complements this data, clearly demonstrating the enhanced efficacy of the targeted system relative to the uncoated control. These observations suggest the potency of this approach to deliver the payload in an efficacious manner to the 143B osteosarcoma solid tumor.

3. Conclusion

LbL is a versatile platform to functionalize nanoparticles in ways that promote improved biological performance. Prior art has established LbL as a means to impart protein-resistive, long-circulating properties to nanoparticle systems, with a means to control biodistribution of both the carrier and drug in a complex systemic environment. This investigation further demonstrates the modularity of this approach to impart targeting capabilities to the nanoparticle to diseased tissue to achieve enhanced treatment outcomes. We capture this potential with the synthesis of osteotropic nanoparticles via incorporation of alendronate-functionalized PAA as a means of surface modification of drug-loaded liposomes. Different nanoparticle core substrates may be used for imaging and treatment for a variety of bone diseases. While surgical resection of a primary tumor will continue to be the first-line of treatment, subsequent treatment with the osteotropic nanoparticles has the potential to decrease recurrance rates and increase successful outcomes. These functional nanoparticles are also highly promising for future investigations towards treatment of bone-localized metastases of invasive cancer cell types such as breast and lung cancer. The potential to further generalize this approach towards the built-to-order manufacture of different targeted delivery systems continues to provide much promise for LbL nanoparticles.

4. Experimental Section

PAA-Alendronate conjugation

Alendronate (Alfa-Aesar) was conjugated to poly(acrylic acid) (Sigma) through the primary amine functional group of alendronate. Half of the free carboxyl end group of the poly(acrylic acid) was targeted for coupling. As both of the reacting species were only soluble in water, we have used water soluble 4-(4,6-Dimethoxy-1,3,5-triazin-2-yl)-4-methylmorpholinium chloride (DMTMM) as the coupling agent[12]. To perform the coupling chemistry, alendronate (1.0 eq.) was added to a solution of poly(acrylic acid) (0.5 equivalents considering all carboxylic groups) in 100 mL water. The solution was stirred for 10 minutes after which DMTMM (2.0 equiv.) was added to the resulting solution. The reaction was allowed to run for 12 hours at room temperature. After the reaction period, the solution was dialyzed against water for 36 hours for complete removal of coupling agent and unreacted alendronate. The dialyzed solution of alendronate-conjugated poly(acrylic acid) was lyophilized to yield a white foam-like product in 65% yield. 1H NMR (in D2O): 1.33 – 1.9 ppm [broad signal, poly(acrylic acid)], 2.10–2.40 ppm [broad signal, poly(acrylic acid)], 2.88 ppm (2H, alendronate). The degree of conjugation was estimated according to the assay protocol reported previously after the hydrolysis of the conjugate at pH 10 with 0.1M NaOH[13]. The estimated degree of functionalization was found to be 43.2%.

LbL on QDs

Carboxyl-modified quantum dots (QD800, Life Technologies) were suspended in dilute solution (~10uL stock in 1mL DI water) and injected in excess 10mL polyelectrolyte (5mg/mL for PLL-Hydrochloride (4–15K, Sigma); 1mg/mL PAA_{450K}-Alendronate) while under agitation at 4°C. Each layer was incubated for ~30 minutes, prior to purification via ultracentrifugation (12,500 RPM, 30m minutes – 1st layer required longer spins, subsequent

purifications are much more expedient) and washing with DI water, repeated twice prior to introduction to the subsequent polyelectrolyte. The final functionalized particle was re-suspended in 1X PBS after the 2nd wash and filtered in a 0.45μm filter for further experimentation.

Liposome synthesis

Liposomes were formulated at a mass ratio of 56:39:5 (DSPC:Cholesterol:POPG – all purchased from Avanti Polar Lipids). These three components were dissolved in a 2:1 mixture of chloroform:methanol. A thin film of these materials was generated by rotary evaporation at 40°C, 150 mbar for approximately 10 minutes. This film was allowed to dessicate overnight for complete drying. Hydration of the lipid film was conducted at 65°C under sonication in 300 mM citric acid buffer (pH 4) for 1 hour, after which they were filtered through a 0.2 μm PES syringe filter and allowed to cool to room temperature. The pH of the liposomal suspension was then adjusted to 6.5 by addition of 300 mM sodium carbonate buffer to create a gradient between the exterior and interior compartments. Doxorubicin (LC Laboratories) at a feed ratio of 3 mg drug to 50 mg lipids was then added in a 0.9% sodium chloride solution to load via a pH gradient method. The final drug-loaded system was subsequently purified out of the high salt buffers and any excess, unloaded drug via centrifugal filtration (100K MWCO Millipore) and transferred to DI water for subsequent functionalization via LbL. Blank liposomes were prepared in the same fashion; however, no drug was added.

LbL on liposomes

Liposomes were diluted in 1 mL DI water (from a 50 mg batch prepared in a final suspension of 5 mL DI water – use ~200 μL stock to 800 μL DI water) and injected in excess polyelectrolyte under agitation at 4°C as previously described for QDs. Incubate for ~30 minutes, purify via ultracentrifugation at 10,000 RPM for ~10 minutes – repeat twice prior to introduction to subsequent polyelectrolyte. The final, functionalized liposomal system was filtered through a 0.45 μm filter and suspended in 1X PBS for further experimentation.

Physicochemical characterization

Dynamic light scattering and zeta potential analysis was conducted in 10 mM sodium chloride at 25°C using a Malvern ZS90 zeta-sizer. High-performance liquid chromatography (Agilent technologies, 1:1 acetonitrile to pH 5 water mobile phase) and nanodrop absorbance measurements (480nm) were performed to quantify doxorubicin concentrations in the prepared samples. Cryo-TEM was conducted by imaging a frozen dilute sample of the liposomal suspension at 120 kV.

In vitro Binding/Cytotoxicity

143B osteosarcoma cells and human mesenchymal stem cells were seeded in 96-well tissue culture plates at a density of $1x10^3$ cells/well and allowed to proliferate for 48 hours. PLL-Cy5.5 labeled particles were quantified based on fluorescence, serially diluted in cell culture media and added to the cells. After 24–48 hours, cells were washed 3X with PBS. Binding

was measured by quantifying the amount of residual fluorescence in the well. Cytotoxicity was measured using a standard MTT assay.

Fluorescence-activated cell sorting analysis

Measurements were performed using a BD LSRFortessa (BD biosciences, San Jose, CA). PLL-Cy5.5 fluorescence was collected following excitation at 640 nm and detected at 710/50 nm (AF700 channel). Cell-association data presented as representative histogram overlays of data collected in triplicate following 143B cell incubation with blank, PLL-Cy5.5 coated, PAA-Alendronate functionalized LbL liposomes for 2 hours at 37°C in 96-well plates. Final samples ran for analysis were washed 3X with optiMEM and trypsinized immediately prior to introduction to the flow cytometer. Blue is the representative treatment; red is the control sample without treatment.

Confocal Microscopy

Images were taken using a Nikon A1R Ultra-Fast Spectral Scanning Confocal Microscope (Nikon instruments Inc., Melville, NY). 143B cells were seeded in a CELLview glass bottom dish (Greiner Bio-One GmbH, Germany) at 1×10^5 cells per well and grown overnight. Cells were then incubated with blank, PLL-Cy5.5 coated, PAA-Alendronate functionalized LbL liposomes (or QDs) for 2 hours at 37°C. At the end of this period, cells were washed, fixed via paraformaldehyde, permeabilized via Triton-1X, and stained with phalloidin-568 for 30 minutes, followed by addition of DAPI for an additional 10 minutes, after which they were washed 3X and imaged.

Xenograft development/targeting/treatment/monitoring – NCR nude

Cells were mixed in a 1:1 ratio with BD Matrigel™ Basement Membrane Matrix to a final density of 5×10^6 cells/0.1 mL injection. 0.1mL injections of the matrix-cell suspension were performed in each rear hind flank of NCR nude mice (Taconic). Tumors were allowed to grow until a visible tumor was established, approximately 25 mm^2 in tumor area prior to treatment (determined via caliper measurements via the longest length and width dimensions); for tumor targeting, xenografts were allowed to grow near terminal size (1 cm in diameter) to reduce effects of EPR. Treatments were injected in 0.1mL 1X PBS at the concentration and treatment regimen indicated in the figure legend. Imaging was performed using whole-animal fluorescence imaging (IVIS, Xenogen, Caliper) at the time points indicated pre- and post-administration at the given fluorescence filters. For targeting experimentation, functionalized, fluorescent systems were administered at a radiant efficiency of ~$3x10^9$ (700 channel)/~$1x10^9$ (800 channel) in a 0.1mL injection. This was determined by imaging the vial prior to injection and diluting as necessary in 1X PBS. Tissue harvest (liver, spleen, kidneys, heart, lungs, tumors, ‘gutted’ skeleton) was performed at the terminal point of the experiment and imaged for fluorescence recovery against an untreated control for auto-fluorescence determination. Tumor sizes for the remediation study were monitored via caliper measurements, whereby areas based on the largest visible length and width dimensions were measured. Depth proved challenging to reliably measure at early time points due to skin thickness, therefore it was not included for a final volume determination for real-time tumor size measurements.

Pharmacokinetics (circulation) – immune-proficient BALB/c

Fluorescent systems (PLL-Cy5.5 coated LbL-targeted empty liposomes) were administered in 0.1mL 1X PBS injections in BALB/c mice (Taconic) at a relative concentration of ~$3x10^9$ (700 channel)/~$1x10^9$ (800 channel) in a 0.1mL injection, based on fluorescence in the IVIS prior to injection. Mice were imaged pre- and post-nanoparticle administration using whole-animal fluorescence imaging (IVIS, Xenogen, Caliper) at the time points indicated and at the given fluorescent filters. Retro-orbital bleeding was performed in a cohort of injected mice to determine the serum half-life of the particles, presented on the basis of fluorescence recovery in these isolated blood samples (~0.1mL blood/time point done in 3 different mice for each time point plotted). Fluorescence recovery was determined by imaging in the IVIS immediately following isolation and dilution 1:1 in EDTA to prevent coagulation. Final data is normalized to an untreated control blood sample to remove artifacts of auto-fluorescence. The data was fit to a two-compartment model (two-phase decay in PRISM®), from which the fast and slow half-lives characterizing the data were extracted.

Histology

Tumors were resected at the terminal point of experimentation and fixed in 4% paraformaldehyde (PFA) for 48 hours and transferred to 70% ethanol until processed. Tissue was embedded in paraffin wax and sections were stained with routine hematoxylin and eosin (H&E) and Masson's trichrome stain.

Statistical Analysis

Experiments were performed in triplicates, or otherwise indicated. Data were analyzed using descriptive statistics, single-factor analysis of variance (ANOVA), and presented as mean values ± standard deviation (SD) from three to eight independent measurements. Statistical comparisons between different treatments were assessed by two-tailed t tests or one-way ANOVA assuming significance at $P < 0.05$.

Supplementary Material

Refer to Web version on PubMed Central for supplementary material.

Acknowledgments

This work was supported by the NIH through grants P30 CA14051 (NCI), 5 U54 CA151884-02 (CCNE), R01 AG029601 (NIA), and R01 EB010246 (NIBIB). The authors acknowledge assistance from the Koch Institute Swanson Biotechnology Center, specifically the Hope Babette Tang (1983) Histology Facility, the Applied Therapeutics and Whole Animal Imaging Facility, and the Flow Cytometry Facility. S.W.M. acknowledges a graduate research fellowship from NSF. Z.J.D. acknowledges a CJ Martin Fellowship from the National Health and Medical Research Council, Australia. P.T.H. acknowledges the David H. Koch (1962) Chair Professorship in Engineering.

REFERENCES

1. Rodan G, Martin T. Science. 2000; 289:1508. [PubMed: 10968781]
2. a) Mundy G. Nat. Rev. Cancer. 2002; 2:584. [PubMed: 12154351] b) Wang D, Miller S, Kopecková P, Kopecek J. Adv. Drug Deliv. Rev. 2005; 57:1049. [PubMed: 15876403]
3. Giger E, Castagner B, Leroux J-C. J. Controlled Release. 2013; 167:175.

4. a) Hengst V, Oussoren C, Kissel T, Storm G. Int. J. Pharm. 2007; 331:224. [PubMed: 17150316] b) Choi S-W, Kim J-H. J. Controlled Release. 2007; 122:24.c) Heller D, Levi Y, Pelet J, Doloff J, Wallas J, Pratt G, Jiang S, Sahay G, Schroeder A, Schroeder J, Chyan Y, Zurenko C, Querbes W, Manzano M, Kohane D, Langer R, Anderson D. Adv. Mat. 2013; 25:1449.d) Ramanlal Chaudhari K, Kumar A, Megraj Khandelwal V, Ukawala M, Manjappa A, Mishra A, Monkkonen J, Ramachandra Murthy R. J. Controlled Release. 2012; 158:470.e) Kiran RC, Abhinesh K, Vinoth Kumar Megraj K, Anil KM, Jukka M, Rayasa SRM. Adv. Funct. Mat. 2012; 22
5. a) David IG, Frank C. J. Phys. Chem. B. 2001; 105b) Schneider G, Subr V, Ulbrich K, Decher G. Nano Lett. 2009; 9:636. [PubMed: 19170551] c) Pattekari P, Zheng Z, Zhang X, Levchenko T, Torchilin V, Lvov Y. Phys. Chem. Chem. Phys. 2011; 13:9014. [PubMed: 21442095] d) Yuk S, Oh K, Cho S, Kim S, Oh S, Lee J, Kim K, Kwon I. Mol. Pharm. 2012; 9:230. [PubMed: 22149139] e) Sexton A, Whitney S-F, Chong P, Zelikin A, Johnston A, De Rose R, Brooks A, Caruso F, Kent S. ACS Nano. 2009; 3:3391. [PubMed: 19824668] f) Zhao Q, Han B, Wang Z, Gao C, Peng C, Shen J. Nanomedicine. 2007; 3:63. [PubMed: 17379170] g) Shutava T, Balkundi S, Vangala P, Steffan J, Bigelow R, Cardelli J, O'Neal D, Lvov Y. ACS Nano. 2009; 3:1877–1885. [PubMed: 19534472] h) Gittins DI, Caruso F. Advanced Materials. 2000; 12:1947.i) Shutava TG, Pattekari PP, Arapov KA, Torchilin VP, Lvov YM. Soft Matter. 2012; 8:9418. [PubMed: 23144650]
6. Decher G. Science. 1997; 277
7. Hyder, MN.; Shah, NJ.; Hammond, PT. Design and Translation of Nanolayer Assembly Processes: Electrochemical Energy to Programmable Pharmacies. In: Decher, G.; Schlenoff, JB., editors. Multilayer Thin Films: Sequential Assembly of Nanocomposite Materials. Second Edition. Weinheim, Germany: Wiley-VCH; 2012.
8. a) Poon Z, Lee J, Morton S, Hammond P. Nano Lett. 2011; 11:2096. [PubMed: 21524115] b) Morton S, Poon Z, Hammond P. Biomaterials. 2013; 34:5328. [PubMed: 23618629]
9. a) Poon Z, Chang D, Zhao X, Hammond P. ACS Nano. 2011; 5:4284. [PubMed: 21513353] b) Yang X-Z, Du J-Z, Dou S, Mao C-Q, Long H-Y, Wang J. ACS Nano. 2012; 6:771. [PubMed: 22136582]
10. Morton SW, Herlihy KP, Shopsowitz KE, Deng ZJ, Chu KS, Bowerman CJ, DeSimone JM, Hammond PT. Adv. Mat. 2013
11. a) Bromberg L. J. Controlled Release. 2008; 128:99.b) Yan X, Gemeinhart R. J. Controlled Release. 2005; 106:198.c) Hu Y, Ding Y, Ding D, Sun M, Zhang L, Jiang X, Yang C. Biomacromolecules. 2007; 8:1069. [PubMed: 17326676]
12. Kunishima M, Kawachi C, Hioki K, Terao R, Tani S. Tetrahedron. 2001; 57:1551.
13. Walash MI, Metwally ME, Eid M, El-Shaheny RN. Chem. Cent. J. 2012; 6:25. [PubMed: 22472190]

Bone-targeted nanoparticles are manufactured via Layer-by-Layer electrostatic adsorption of an alendronate-functionalized polyelectrolyte, poly(acrylic acid), on a nanoparticle substrate. High levels of bone specificity and efficacy against an osteosarcoma xenograft tumor model demonstrate this approach as an attractive, modular method for designing systems with tissue specificity for enhanced treatment outcomes.

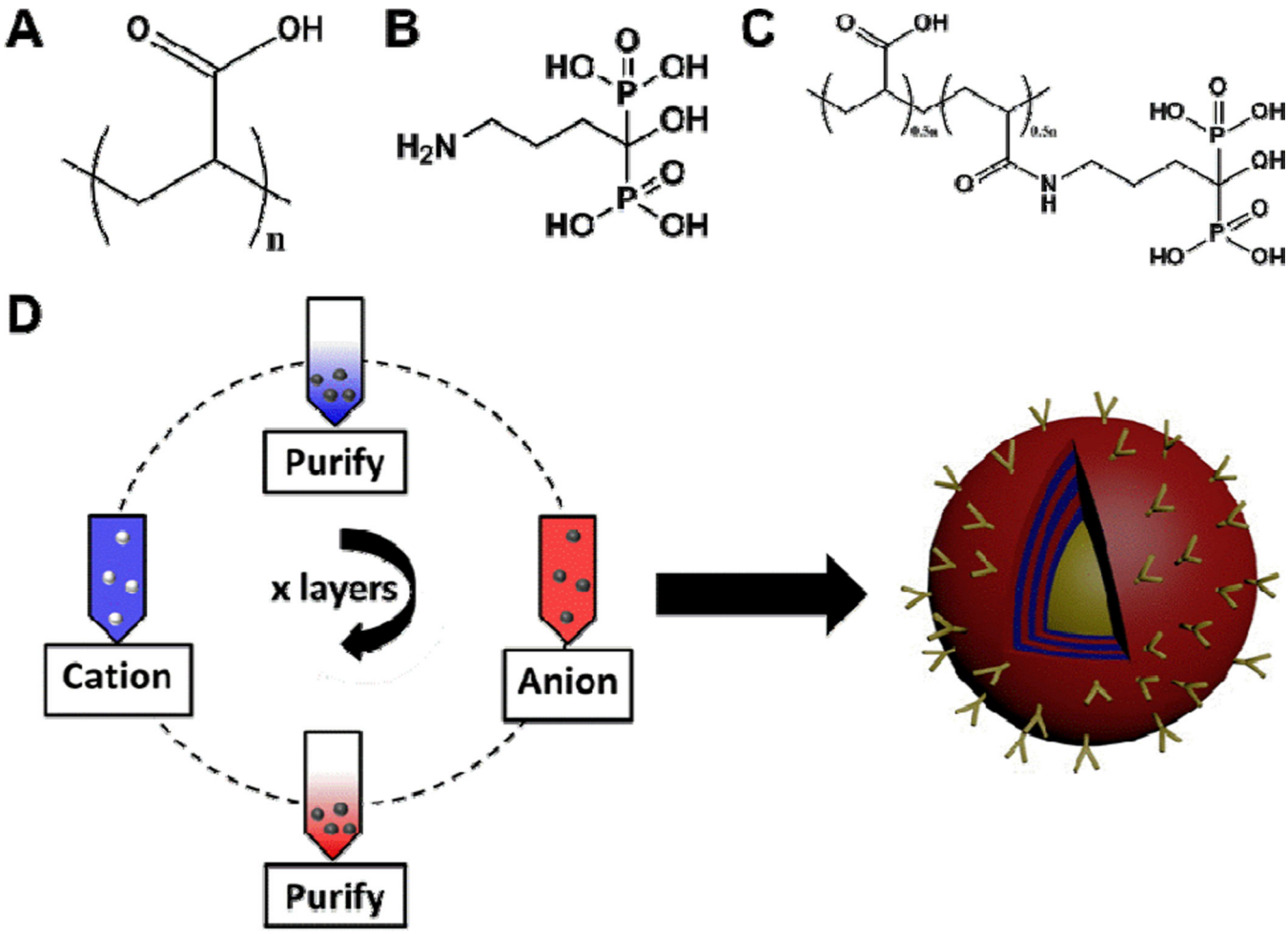

Figure 1. Achieving bone tissue level specificity of LbL coated nanoparticles

(A) Aqueous anionic polyelectrolyte, poly(acrylic acid) [PAA, MW 450K], functionalized with the **(B)** bisphosphonate targeting moiety, alendronate [for high specificity to hydroxyapatite in bone], to yield **(C)** the aqueous, ligand-functionalized polymer at 40% side-chain functionalization (Figure S1), which is used for complementary, iterative adsorption to the polycationic component (poly-L-lysine, PLL) in the film on the NP substrate, schematically illustrated in **(D)**.

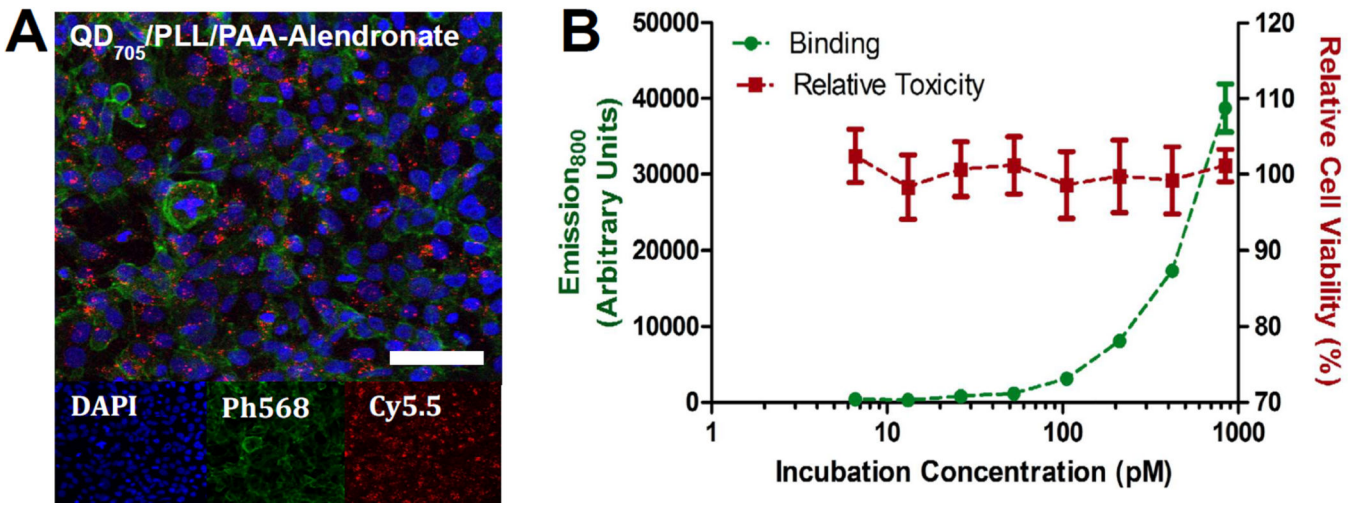

Figure 2. *in vitro* assessment of LbL-targeted QD NPs incubated with 143B osteosarcoma cells

(A) Confocal microscopy of 143B cells incubated with the LbL-targeted QD_{705} core NPs for 2 hours. Blue staining representative of a Hoescht nuclear stain, green representative of a phalloidin stain of the actin filamentous cell structure, and red representative of the nanoparticle fluorescence (QD_{705} fluorescence). Scale bar representative of 20μm. **(B)** Binding and relative cytotoxicity of 3 bilayer [PLL/PAA-Alendronate] LbL-targeted QD_{800} core NPs following incubation for 2 hours in 143B cells. Fluorescence emission data corresponds to that of the nanoparticle core (QD_{800}).

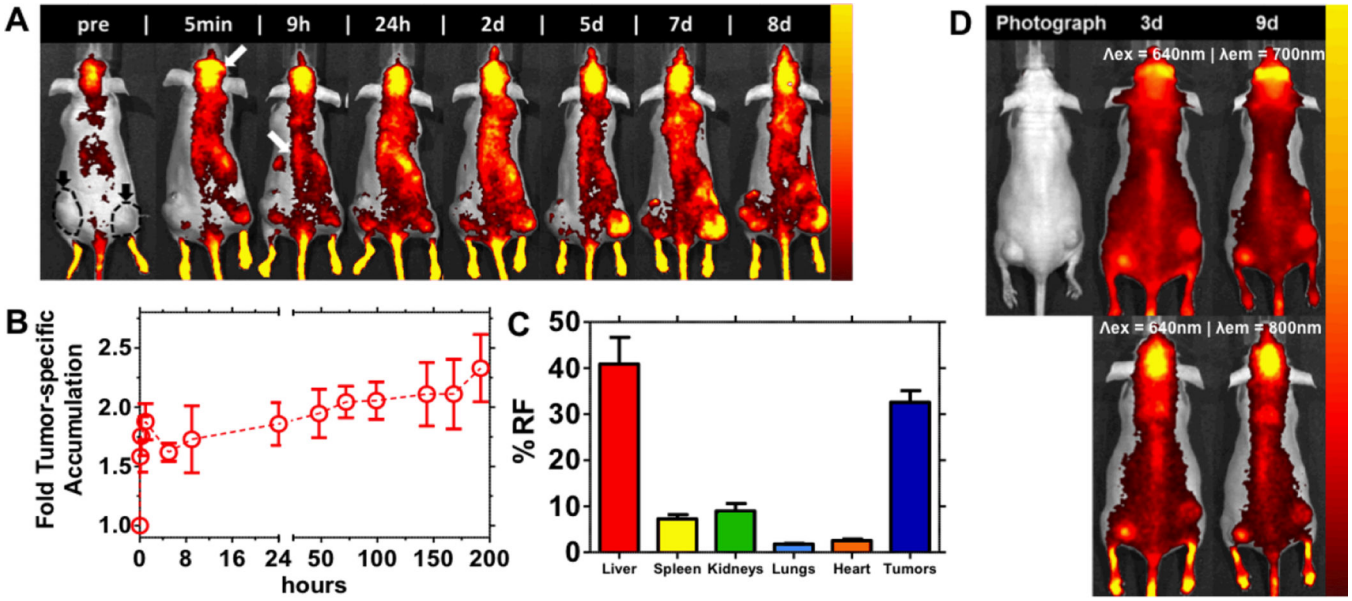

Figure 3. *in vivo* evaluation of LbL-targeted QD_{800} core NPs

(A) Representative live-animal imaging of LbL-targeted QD_{800} core NPs following systemic administration to 143B osteosarcoma xenograft-bearing NCR nude mice. Imaging conducted at λ_{ex} = 640 nm, λ_{em} = 800 nm for up to 8 days. Hind-flank xenografts identified in the pre-injection image; arrows at 5 minutes and 9 hours indicate binding to native bone tissue. **(B)** Quantification of fold tumor-specific accumulation normalized to tissue auto-fluorescence pre-injection for the systemically administered LbL-targeted QD_{800} core NPs, as visualized in **(A)**. n = 3 mice (6 tumors); data presented as mean +/− SEM. **(C)** Biodistribution data corresponding to endpoint of **(A)** (quantified as percent recovered fluorescence following harvest of relevant tissue after 8 days post-administration). n = 3 mice (6 tumors); data presented as mean +/− SEM. **(D)** Co-localization of QD_{800} NP core with LbL-film containing labeled PAA-Alendronate$_{700}$; top row [PAA-Alendronate$_{700}$ channel] – imaging conducted at λ_{ex} = 640 nm, λ_{em} = 700 nm, bottom row [QD_{800} channel] - imaging conducted at λ_{ex} = 640 nm, λ_{em} = 800 nm.

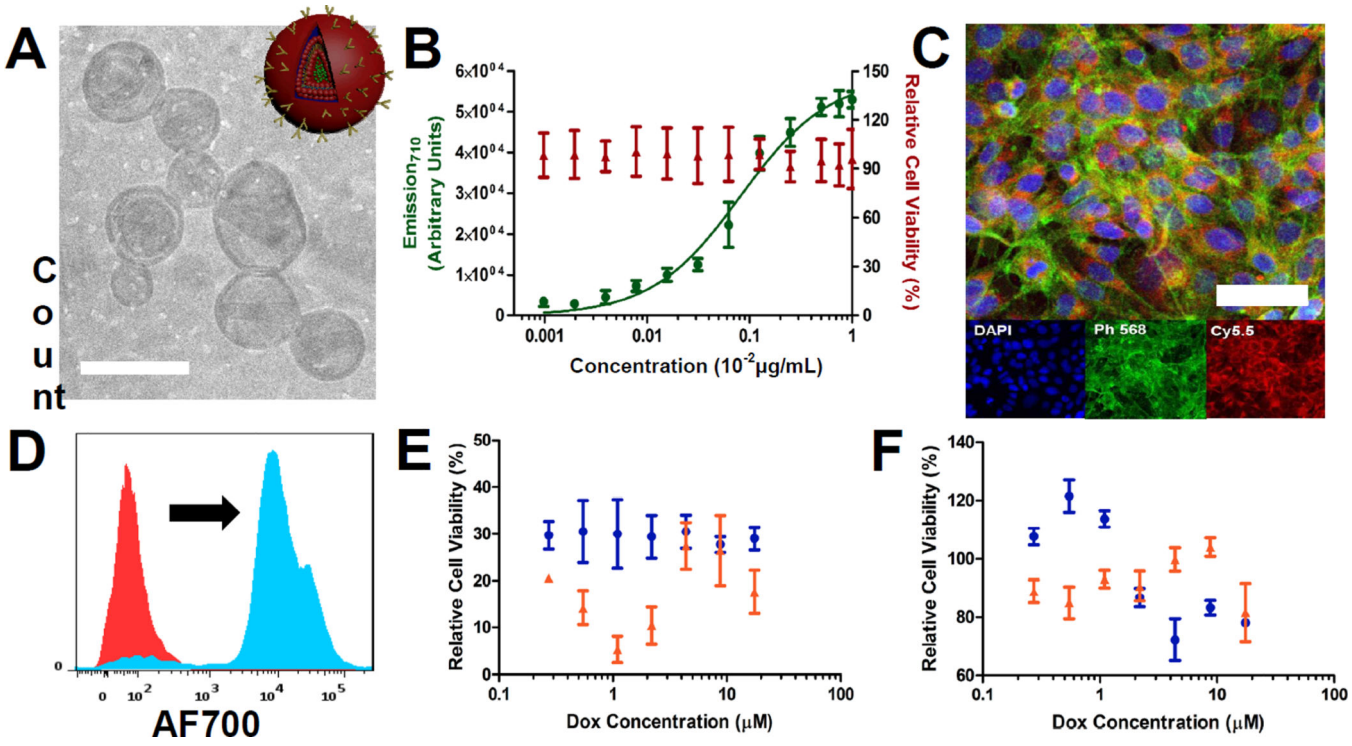

Figure 4. *in vitro* evaluation of LbL-targeted liposomal NPs in 143B cells

(A) Cryo-TEM of LbL-targeted doxorubicin-loaded liposomal NPs. Scale bar representative of 200 nm. **(B)** Binding (2 hour incubation) and relative cytotoxicity (48 hour incubation) of LbL-targeted empty liposomal NPs over a range of concentrations, based on fluorescence, in 143B cells (λ_{ex} = 675 nm, λ_{em} = 710 nm; tracked using PLL_{700} as cationic component in LbL film). **(C)** Confocal microscopy of 143B cells incubated with the LbL-targeted empty liposomal NPs [tracked via PLL_{700} polycationic component in LbL film] for 2 hours. Blue staining representative of a Hoescht nuclear stain, green representative of a phalloidin stain of the actin filamentous cell structure, and red representative of the nanoparticle fluorescence ($PLL_{Cy5.5}$ polymer shell fluorescence). Scale bar representative of 10 µm. **(D)** Representative cell-associated NP fluorescence following a 2 hour incubation of 143B cells with the LbL-targeted empty liposomal NPs. **(E)** *in vitro* cytotoxicity of LbL-targeted doxorubicin-loaded liposomal NPs and the corresponding **(F)** uncoated doxorubicin-loaded liposomal control following 48 hour (blue) and 72 hour (red) incubation periods over a range of doxorubicin concentrations.

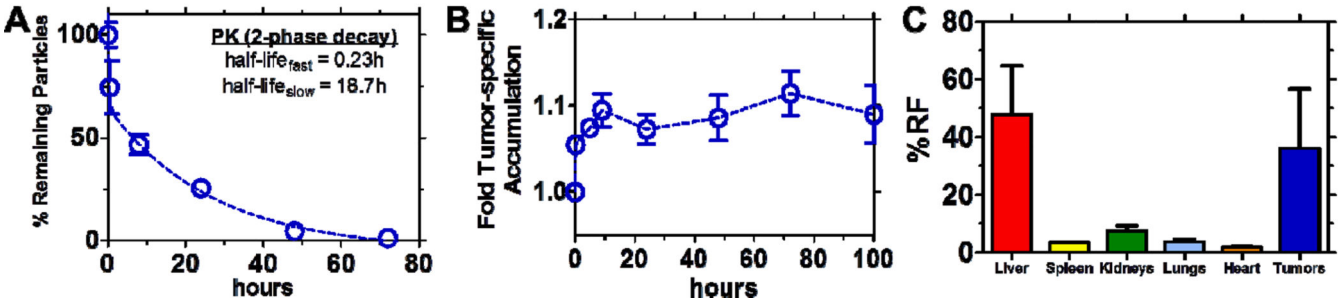

Figure 5. Biological evaluation of LbL-targeted empty liposomal NPs

LbL-targeted empty liposomal NPs tracked via PLL_{700} polycationic component in surface coating. Circulation data in **(A)** normalized to % remaining particles recovered, on the basis of fluorescence [λ_{ex} = 640 nm, λ_{em} = 700 nm], immediately following systemic administration to immune proficient BALB/c mice; data presented as mean +/− SEM (n = 3). Two-compartment model fit to determine half-lives displayed. Data includes background subtraction of blood auto-fluorescence. **(B)** Quantification of fold tumor-specific accumulation normalized to tissue auto-fluorescence pre-injection for the systemically administered LbL-targeted blank liposomal core NPs to 143B xenograft-bearing NCR nude mice; data presented as mean +/− SEM (n = 3). **(C)** Biodistribution data corresponding to endpoint of **(B)** (quantified as percent recovered fluorescence [λ_{ex} = 640 nm, λ_{em} = 700 nm] following harvest of relevant tissue after 100 hours post-systemic administration); data presented as mean +/− SEM (n = 3).

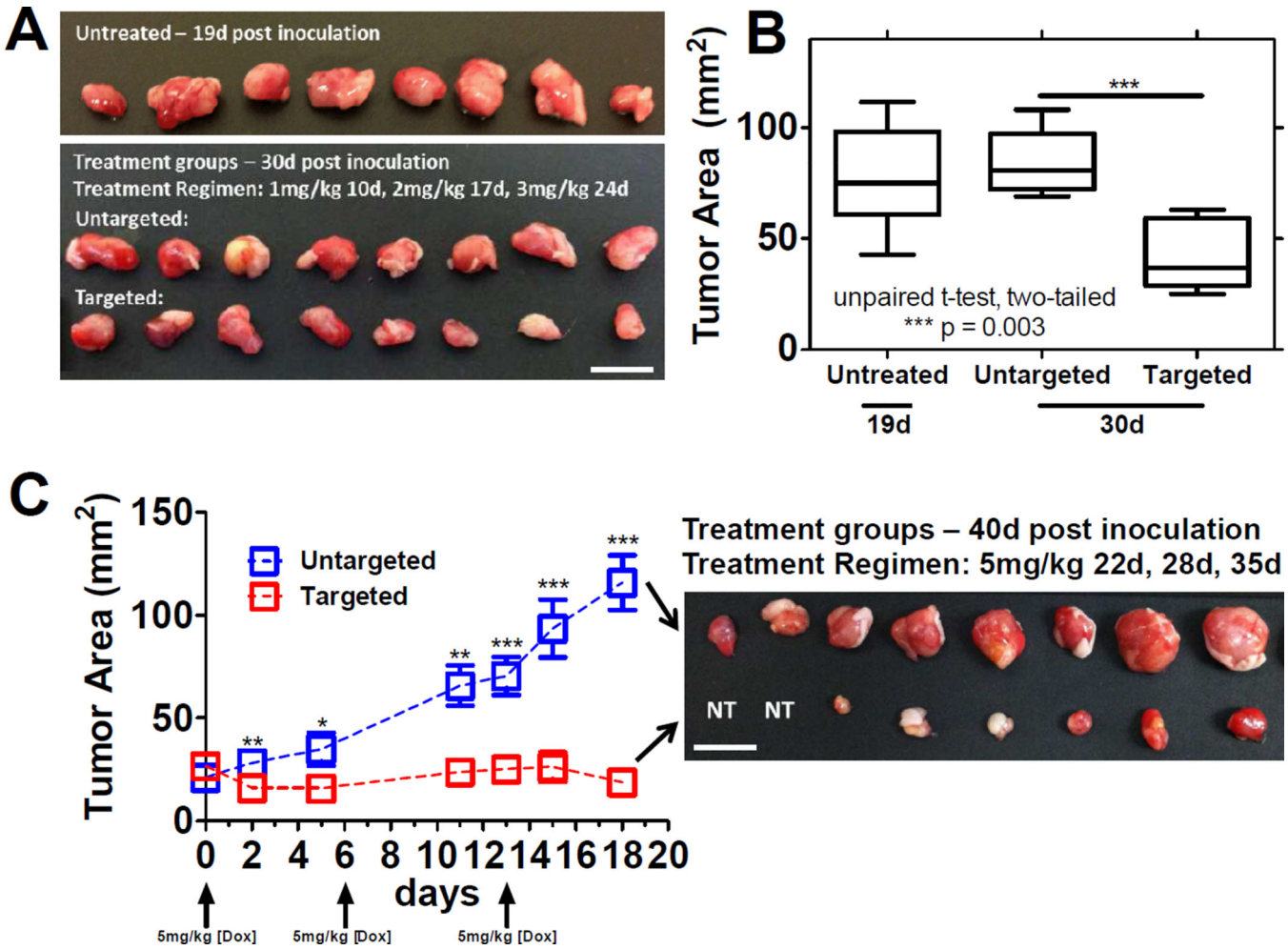

Figure 6. 143B xenograft tumor remediation following treatment with doxorubicin-loaded liposomal formulations

(A) *in vivo* tumor remediation of 143B xenografts in NCR nude mice for LbL-targeted doxorubicin-loaded liposomal NPs, against untreated and uncoated doxorubicin-liposomal NPs. Untreated control xenografts were sacrificed 19 days post-inoculation of xenograft due to tumor burden exceeding 1 cm. Untargeted and targeted Dox-liposomal formulations were sacked at 30 days post-inoculation following a dose-escalation study with the following treatment regimen: day 10 at 1 mg/kg, day 17 at 2 mg/kg, day 24 at 3 mg/kg. Terminal point shown with final tumor area displayed in **(B)**. Statistics are from an unpaired t-test, two-tailed to compare the untargeted and targeted formulations at each time point. Data presented as mean +/− SEM; n = 4. **(C)** Caliper measurements for *in vivo* tumor remediation with repeated dosing of 5 mg/kg for both targeted and untargeted formulations at 22 days, 28 days, and 35 days post-inoculation (displayed as day 0, day 6, and day 13 in **(C)**). Statistics are from an unpaired t-test, two-tailed to compare the untargeted and targeted formulations; *p < 0.05; **p < 0.01; ***p < 0.001. Data presented as mean +/− SEM; n = 4. Resection of tumors from terminal point of **(C)**, n = 4 for each group, displayed from the final caliper measurement.

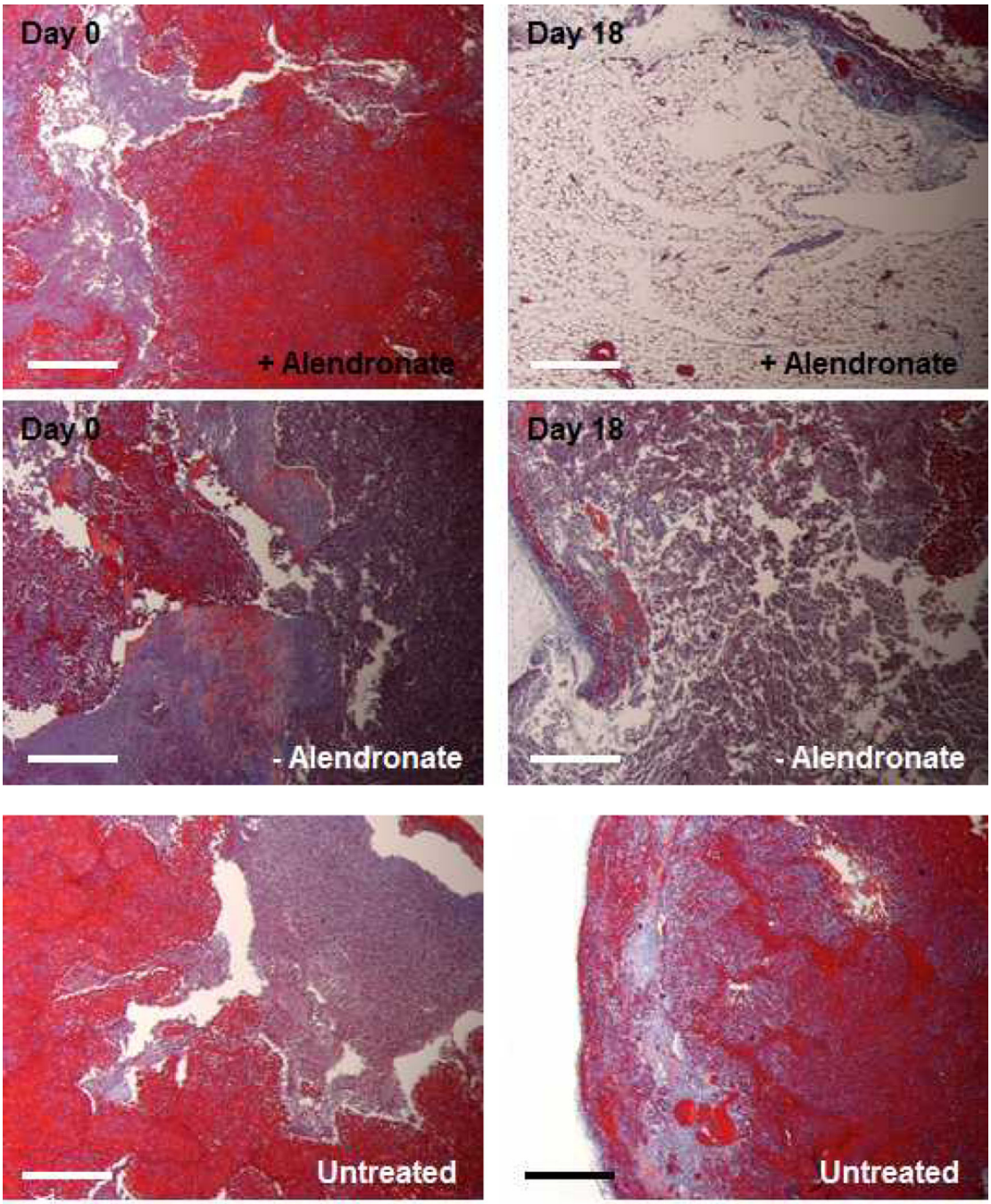

Figure 7.

Representative histology of 143B tumors harvested at 18 days post-treatment corresponding to the terminal point in Figure 6C. (**left column)** tumors prior to treatment; (**right column)** tumors at the 18 day terminal point post treatment of 3 repeated injections at 5 mg/kg doxorubicin. **(top row)** tumors treated with PAA-Alendronate coated doxorubicin-loaded liposomes, **(middle row)** uncoated dox-loaded liposomes, and **(bottom row)** untreated

animals. Masson's trichrome stain – red = 143B osteosarcoma cells, blue = connective tissue; scale bars representative of 100 μm.